

## Original papers

## Deciphering the UAV-LiDAR contribution to vegetation classification using interpretable machine learning



Tao Huang<sup>a,g</sup>, Lei Jiao<sup>a,g,\*</sup>, Yingfei Bai<sup>b</sup>, Jianwu Yan<sup>a,g</sup>, Xiping Yang<sup>a,g</sup>, Jiayu Liu<sup>a,g</sup>, Wei Liang<sup>a,g</sup>, Da Luo<sup>c</sup>, Liwei Zhang<sup>a,g</sup>, Hao Wang<sup>a,g</sup>, Zhaolin Li<sup>d,e</sup>, Zongshan Li<sup>d,e,f</sup>, Ni Ji<sup>h</sup>, Guangyao Gao<sup>d,e,f,\*\*</sup>

<sup>a</sup> School of Geography and Tourism, Shaanxi Normal University, Xi'an 710119, China

<sup>b</sup> Laošan State-owned Forest Management Bureau, Yan'an 716100, China

<sup>c</sup> Yulin University, Yulin 719000, China

<sup>d</sup> State Key Laboratory of Urban and Regional Ecology, Research Center for Eco-Environmental Sciences, Chinese Academy of Sciences, Beijing 100085, China

<sup>e</sup> National Observation and Research Station of Earth Critical Zone on the Loess Plateau in Shaanxi, Xi'an 710061, China

<sup>f</sup> Shaanxi Yan'an Forest Ecosystem Observation and Research Station, Beijing 100085, China

<sup>g</sup> Shaanxi Observation and Research Station for Ecology and Environment of Desert-Loess Zone at Yulin, Xi'an 710119, China

<sup>h</sup> Shangluo Agricultural Products Quality and Safety Center, Shangluo 726000, China

## ARTICLE INFO

## Keywords:

LiDAR

RF

GEE

Vegetation classification

SHAP

## ABSTRACT

Accurate classification of land cover types is a prerequisite for the protection of natural ecosystems. In particular, understanding the spatial distributions of different vegetation types is essential for the effective management, monitoring, and conservation of forest ecosystems. Satellite remote sensing uses rich spectral band information for land cover classification, but it is usually insufficient for high-precision vegetation classification work in small areas. However, the structure and vegetation information provided by Aerial LiDAR Scanning (ALS) can significantly increase the classification accuracy. To address these limitations, this study utilized high-resolution unmanned aerial vehicle (UAV) imagery and aerial LiDAR point cloud data to improve the accuracy of vegetation classification and plantation observation at the catchment scale. Using Google Earth Engine (GEE), spectral, textural, and LiDAR-derived topographic and vegetation features are extracted and integrated, followed by supervised classification using Random Forest (RF) and Support Vector Machine (SVM) models. This approach enhances the accuracy and efficiency of vegetation classification at the catchment scale. The classification results of SVM and RF demonstrated that incorporating LiDAR-derived topographic and vegetation features significantly improved the classification accuracy compared to using spectral and textural features only. Specifically, the overall accuracy (OA) of the RF classification increased from 94.37 % to 99.36 %, while the kappa coefficient improved from 91.08 % to 99.01 %. Moreover, the impact threshold analysis based on SHAP values showed that canopy height, tree density, and elevation were the top three key features driving the improvement in the classification performance. This study offers new insights and methods for vegetation classification in complex ecological environments.

## 1. Introduction

Protection of ecosystems and the services they provide while meeting the ever-growing demands of humanity is a core long-term challenge in achieving sustainable development (Lambin & Meyfroidt, 2011). Accurate differentiation of land cover types is vital for effective protection

of natural ecosystems. Land cover changes are both a cause and consequence of global climate change, influencing energy balance and biogeochemical cycles. In particular, tree species composition and spatial distribution, are crucial for the management of forest and land resources, biodiversity conservation, food security, and forest carbon storage, among other applications (Yue et al., 2020). To facilitate in-

\* Corresponding author at: School of Geography and Tourism, Shaanxi Normal University, Xi'an 710119, China.

\*\* Corresponding author at: State Key Laboratory of Urban and Regional Ecology, Research Center for Eco-Environmental Sciences, Chinese Academy of Sciences, Beijing 100085, China.

E-mail addresses: [ljiao@snnu.edu.cn](mailto:ljiao@snnu.edu.cn) (L. Jiao), [gygao@rcees.ac.cn](mailto:gygao@rcees.ac.cn) (G. Gao).

depth research on the diverse and complex impacts of ecosystems under different vegetation types, it is vital to improve the accuracy and reliability of vegetation classification models (Qin et al., 2022). Remote sensing technologies, are increasingly being utilized for species classification, tree height mapping, and estimation of aboveground biomass and carbon storage in forests (Oehmcke, 2024). Advanced remote sensing methods for species classification not only enhance carbon stock monitoring but also contribute significantly to economic, ecological, and forest management and planning (Fernández-Martínez et al., 2014).

Studies on the applications of remote sensing for monitoring land cover changes are evolving and have achieved increasing spatial, temporal and spectral resolution. In recent years, many researchers have explored the use of high spatial resolution imagery, such as IKONOS, QuickBird, and Sentinel-2A, for applications such as land use/land cover classification at the regional scale (Cao et al., 2021). However, these satellites are insufficient for accurate monitoring and analysis at small scales, such as catchment scale. Owing to their high-resolution and multispectral data collection capabilities, drone-based observation methods are affected by sunlight conditions and temperature. Consequently, they are not suitable for all-weather operation, and their advantages are limited by areas with dense vegetation, such as forests, where high vegetation cover hinders effective structural data acquisition (Fauvel et al., 2013). Under these circumstances, the new generation of active remote sensing technology, namely, LiDAR, has proven to be an effective tool for capturing complex three-dimensional forest structure information (Li et al., 2024). However, in areas with complex vegetation compositions and heterogeneous topographies, high-precision classification can no longer rely solely on spectral characteristics. The structural and vegetation information provided by UAV-borne LiDAR, which offers a low-cost and flexible approach, can significantly increase the accuracy of identification. For example, Corte et al. (2020) predicting individual tree attributes by high-density UAV-Lidar and machine learning. Hyperspectral imagery and point clouds obtained with LiDAR or through Structure from Motion algorithm (SfM) were applied to discriminate healthy from diseased plants (Caras et al., 2024). Torabzadeh et al. (2019) integrated imaging spectroscopy (IS) data with Airborne Laser Scanning (ALS) data, and demonstrated that structural features such as vegetation height, cumulative density, and point density could improve the accuracy of temperate mixed forest tree species mapping. These studies revealed that LiDAR can be beneficial in retrieving the vegetation canopy attributes to improve the accuracy of vegetation types classification.

As discussed in various studies, the usefulness of LiDAR data has been increasingly recognized by researchers worldwide, many recent studies have focused on deriving more complex predictive variables from LiDAR data, not only by integrating passive optical information with LiDAR-derived Canopy Height Model (CHM) data but also by incorporating variables that describe canopy morphology. (Fassnacht et al., 2016; Li et al., 2024; Wang, 2024). Despite the continuous progress of LiDAR technology, vegetation classification still faces challenges, particularly in extracting plants and tree structural features such as tree height and crown spread (Corte et al., 2020). To overcome this challenge, researchers have proposed a number of LiDAR indicators. Fernández-Martínez et al. (2014) explored the effects of forest type, age, management and nitrogen deposition. Their findings indicated that, in addition to standard parameters, other variables, such as topographic features (elevation, slope, and aspect) and climatic variables (temperature and precipitation), also influence forest growth. Features such as tree height, crown diameter, partial canopy cover, leaf area index, and biomass are commonly estimated using ALS (Airborne Laser Scanning) data. Additionally, LiDAR waveform data can enhance classification accuracy, even though their capacity for extensive complex tree species classification is still limited (Hovi, 2014). However, it remains unclear which specific LiDAR metrics are most important for tree species classification and how intrinsic morphological differences between species are reflected in these metrics. Moreover, an effective theoretical

framework for the integration of LiDAR features with optical imagery has not been fully developed according to studies above. Therefore, it is necessary to explore the potential of combining high-resolution optical imagery with LiDAR data to improve tree species classification accuracy. This includes investigations of novel LiDAR-derived feature metrics that may contribute to increased precision.

The advantages of machine learning algorithms in handling complex data structures have led to rapid growth in research on supervised classification over the past two decades, particularly in the use of the Random Forest (RF) method. RF is widely favoured due to its strong capability to process large datasets and high-dimensional data, produce reliable classification results, and rank the importance of input variables for classification outcomes (Belgiu, 2016). Ning employed neural networks for pixel-based classification across six different scenarios, achieving an accuracy of 96.6 % by incorporating texture, terrain, and phenological features (Ye, 2022). Qin et al. (2022) combined structural, spectral, and textural features to train an RF classifier, demonstrating promising results for individual tree segmentation and species classification in subtropical broadleaf forests. Thus, machine learning methods show substantial potential for exploring the complex relationships between tree species classification targets and all potential feature metrics that contribute to classification, such as spectral variables, textural variables, and LiDAR-derived features. This potential can be leveraged for high-precision tree species classification mapping as well as studies on the contributions of influencing variables.

Motivated by the above background, this study aims to explore the contribution of LiDAR-derived topographic and vegetation features to improving the accuracy and efficiency of vegetation classification at the catchment scale on the Loess Plateau. It integrates high-resolution spectral features, textural features, and LiDAR-derived features from UAVs, using machine learning models and the interpretable SHAP algorithm. The specific objectives of this study are: (1) to establish a refined vegetation classification method based on high-resolution UAV data and LiDAR data, (2) to identify key LiDAR-derived indicators to provide feature selection references for high-precision vegetation classification on fragmented surfaces of loess hills and gully regions, and (3) to comprehensively compare the classification accuracy of different algorithms and visualize the threshold variations of sub-feature contributions to different vegetation classes in classification..

## 2. Materials and methods

### 2.1. Study area and field measurements

The Yangjuangou catchment in Liqu Town ( $36^{\circ}41' - 36^{\circ}42'N$ ,  $109^{\circ}30' - 109^{\circ}31'E$ ), located northeast of Baota District, Yan'an City, Shaanxi Province, was selected as our experimental area (Fig. 1). It is a secondary tributary of the Yanhe River and a primary tributary of the Nianzhuanggou catchment. The total area of the catchment is  $2.02 \text{ km}^2$ , and is characterized by loess ridges and gullies, with a gully density of  $2.74 \text{ km/km}^2$ . This region is representative of the geomorphological features of the Loess Plateau gully region, which has poor erosion resistance, leading to severe soil erosion exacerbated by human activities. The area serves as a transitional zone between forest and grassland (Wang et al., 2018). Based on LiDAR data, the elevation ranges from 1008 to 1229 m. Influenced by a semiarid continental monsoon climate, the area experiences significant interannual variation in precipitation, which is predominantly concentrated between July and October.

Owing to the significant destruction of natural vegetation by human activities, the region is now covered mainly by artificial secondary vegetation, including trees, shrubs, and herbs, that were planted after the implementation of the Grain for Green Project (Liu et al., 2024). The land cover is highly diverse, and comprises vegetation (arbour, shrubs, and herbs), arable land (dams and terraces), residential areas, roads (cement and dirt roads), and water bodies (Wang et al., 2018). Previous studies have examined the temporal and spatial changes in the land use/

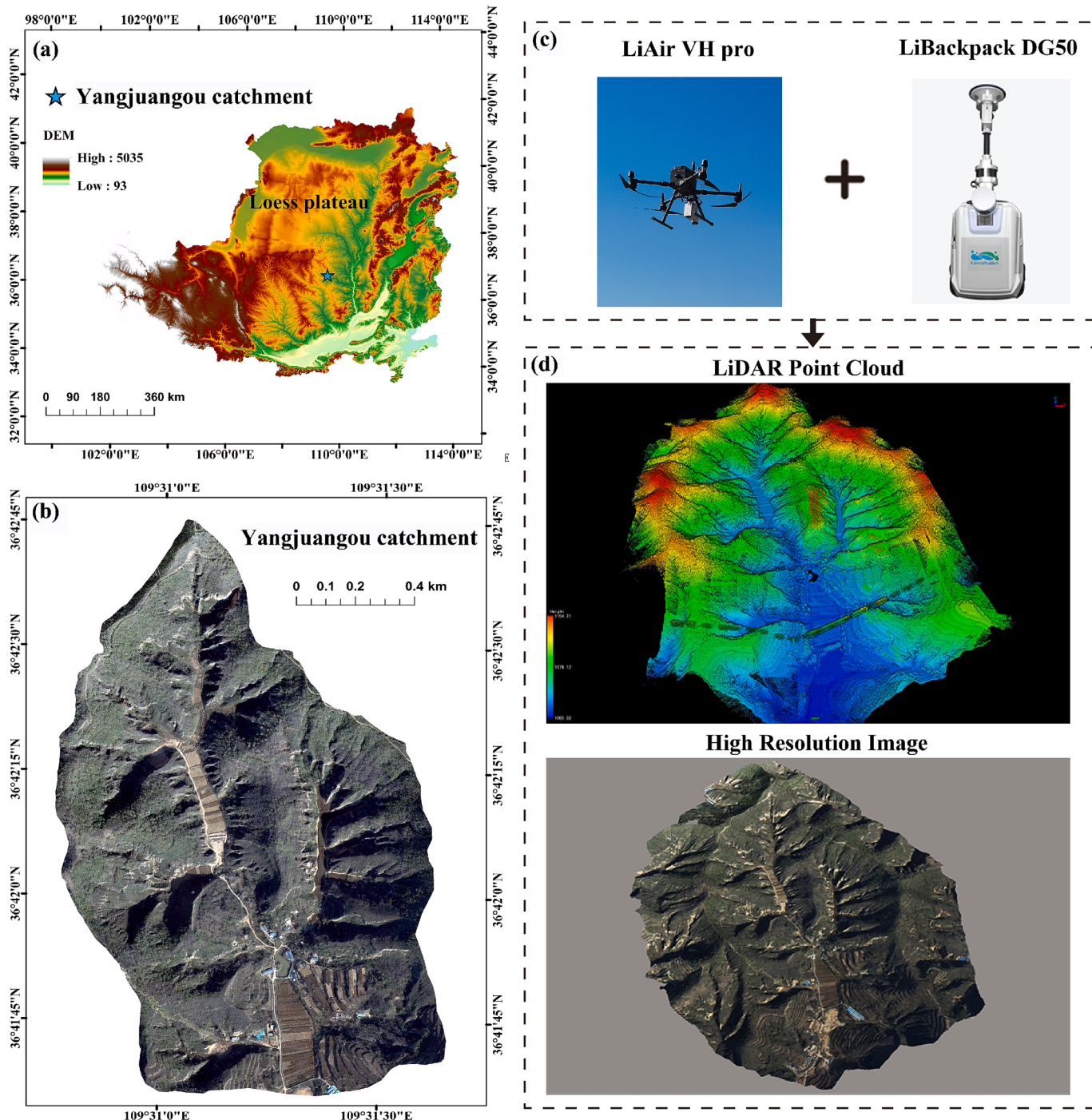


**Fig. 1.** (a) Location of the Yangjuangou catchment; (b) DSM of the Yangjuangou catchment; (c) Airborne LiDAR and backpack radar equipment; (d) LiDAR point and high-resolution imagery data. The projection coordinate system used for all of the data in this study is WGS 1984 UTM Zone 49N.

cover in this area. This provides a firm foundation for, integrating UAV high-resolution image data and LiDAR point cloud data to test the classification accuracy of different feature combinations in this region.

## 2.2. Data collection and preprocessing

### 2.2.1. Uav-borne high-resolution imagery data

UAV-borne digital aerial photography of the entire study area was conducted using a DJI Matrice 300 hexacopter UAV (Shenzhen DJI Innovations Co., Ltd., China) equipped with a Hasselblad camera. This camera features a 20-megapixel lens and a 1-inch CMOS sensor (sensor size: 8.8 mm × 24 mm), with a maximum photo resolution of 5472 ×

3648 pixels. High-resolution images of the study region were captured during clear midday weather conditions on October 2020, covering an area of approximately 2.02 km<sup>2</sup> with a spatial resolution of 0.1 m. Given that the entire study area is a part of the hill and gully topography of the Loess Plateau (Cheng, 2023), the aerial survey flight speed was set at 10 m/s, with the flight altitude maintained at 400 m. Images are captured according to a standard of no less than 80 % forward and lateral overlap, and are stitched to produce true-colour images. Orthophoto correction was completed using the Context Capture software, and the orthophotos were projected using the WGS1984 reference ellipsoid and UTM Zone 49 N projection. Fig. 2 shows field photographs of the three vegetation types, *Robinia pseudoacacia* (RP), *Armeniaca sibirica* (AS) and herbs and

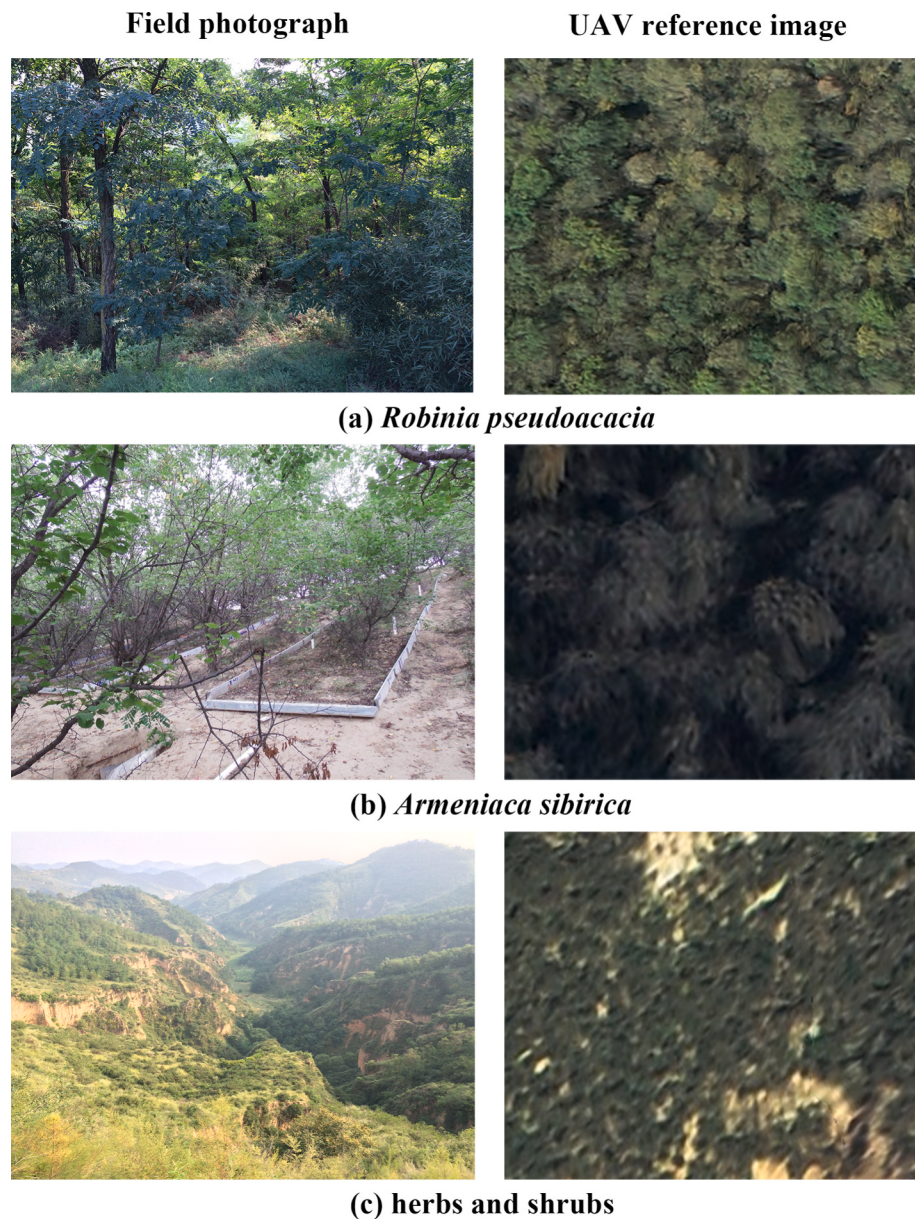


**Fig. 2.** Field photographs of three vegetation species and their UAV reference images.

shrubs (HS), as well as views of the corresponding UAV imagery.

#### 2.2.2. Uav-borne LiDAR point cloud data

The LiDAR data utilized in this study were collected on October 19, 2020, using the LiAir VH pro LiDAR system developed by Beijing Digital Greenland Technology Co., Ltd., China. This advanced system integrates a lightweight LiDAR sensor, an inertial navigation system, and a control system and was deployed using a DJI Matrice 300 hexacopter UAV (Shenzhen DJI Innovations Co., Ltd., China). The UAV performed terrain-following scans at an altitude of 80 m above the DEM model, flying at speeds ranging from 5 to 10 m/s. The system operated with a field of view of  $70.4^\circ$  (horizontal)  $\times$   $77.2^\circ$  (vertical), and a laser wavelength of 905 nm. The initial raw data were subjected to preprocessing to produce a LiDAR point cloud with an overall average density better than 20 points per square metre. Moreover, some ground-based backpack radar scanning work was incorporated using the Libackpack DG50 system to encrypt sparse areas of the ground point cloud in addition to airborne LiDAR scanning. The final denoised point cloud dataset exceeds 15 GB in size and covers an area of over 2.2 square kilometers. This

dataset serves as one of the fundamental data sources for vegetation classification. The preprocessing process primarily involves the integration and resolution of IMU data, airborne GPS data, base station GPS data, and laser ranging data to obtain high-precision three-dimensional point clouds.

#### 2.3. Feature extraction

##### 2.3.1. Spectral and textural feature extraction

Spectral features are obtained by linear or non-linear calculations among different bands, which are used to distinguish between feature reflectance differences (Fauvel et al., 2013). The spectral curves of the six land covers are shown in Fig. S1. Notably, all vegetation types exhibited distinct reflectance differences within the visible spectral range. The rural construction area has the highest spectral reflectance in the entire visible wavelength band. RP and water body show high similarity in their spectral reflectance trends, while the AS reflectance significantly lower. As shown in Fig. S1, these six land covers can be distinguished on the basis of their spectral curve differences in the

visible wavelength range. This study primarily uses information from the red (700 nm), green (550 nm), and blue (470 nm) bands of the true-colour images as the spectral features.

However, classification maps derived solely from spectral features are often affected by salt-and-pepper noise. This is because pixelwise classifiers rely only on spectral information and do not consider the spatial dependencies of adjacent pixels within the same class. To increase the classification accuracy and smoothness of classification maps, spectral-spatial classification has gained considerable attention (Fauvel et al., 2013). Texture is a fundamental low-level spatial feature in remote sensing imagery that aids in distinguishing structural details within an image and is widely used for identifying and differentiating spatial patterns in digital imagery (Chrysafis et al., 2019). The resulting gray values in the output image represent the local texture characteristics of the input image (Zhang, 1999). Texture analysis involves computing the gray-level relationships between a pixel and its neighboring pixels based on specific texture metrics, such as mean, standard deviation, contrast, correlation, energy, and entropy. The textural features of remote sensing images, as auxiliary features to spectral characteristics, play a significant role in image analysis and automatic land cover identification. Compared to low-resolution remote sensing images, high-resolution remote sensing images contain more land cover details, providing more textural information. This information is crucial for image classification and is key to resolving the issue of spectral homogeneity among different land covers (Zhu et al., 2024). Therefore, this study aims to efficiently integrate spatial textural information and spectral information into the pixel classifier using the Google Earth Engine platform in conjunction with the spectral-spatial approach of the grey-level co-occurrence matrix (GLCM) (Zhang, 1999). Specifically, eight textural features corresponding to the RGB bands were extracted: mean, variance, homogeneity, dissimilarity, contrast, entropy, correlation, and angular second moment.

### 2.3.2. LiDAR-derived topographic index extraction

The terrain toolbox in LiDAR 360 (Beijing Digital Greenland Technology Co., Ltd., China) was used to preprocess the point cloud data to generate a Digital Elevation Model (DEM) for the Yangjuangou catchment, with a pixel size of  $0.5 \times 0.5$  m. Basic topography indices, including elevation, slope, and aspect, were calculated using the spatial analyst tools in ArcGIS (Fig. S2). Additionally, the topographic wetness index (TWI) was calculated via the raster calculation. The TWI is a physical indicator of the influence of regional topography on the runoff flow direction and accumulation, helping to identify rainfall runoff patterns, areas of potential soil moisture increase, and water accumulation areas. It is one of the most widely used topographic indicators and is related to the spatial distribution and size of runoff saturation areas or variable source areas. TWI is computed from the specific catchment area ( $\alpha$ ) of the upslope slope and the local slope ( $\tan\beta$ ) (Seibert et al., 2007). Direct Insolation (DI) was calculated using the Area Solar Radiation tool in ArcGIS, with the unit of measurement being watt-hours per square metre ( $W/m^2$ ). The solar radiation analysis tool calculates sunlight within a study area or at specific locations. The total radiation calculated for specific locations or areas is presented as the total radiation. For each feature location or position within each terrain surface, direct sunlight, scattered sunlight, and total sunlight are repeatedly calculated to generate a solar radiation map for the entire geographical area.

### 2.3.3. LiDAR-derived vegetation index extraction

The airborne LiDAR point cloud data of the Yangjuangou catchment was first processed using LiDAR360 (Beijing Digital Greenland Technology Co., Ltd., China) for noise removal, ground point classification, DEM, DSM extraction, and calculation of the Canopy Height Model (CHM). The CHM (Fig. S2a), defined as the average height of the vegetation canopy top, was used to identify and segment individual trees using the catchment segmentation algorithm (Chen et al., 2006), obtaining information such as tree positions, tree heights, crown

diameters, crown areas, and tree boundaries. Individual tree segmentation based on the CHM generated the vegetation canopy boundary grid. LAI is one of the most fundamental parameters representing the canopy, structure and is defined as half of the total leaf area per unit ground area. It directly represents the canopy structure and affects energy exchange, evapotranspiration, and carbon dioxide exchange between plants and the atmosphere, making it useful for predicting primary productivity and crop growth (Gower et al., 1999). Canopy Cover (CC) is the percentage of the ground area covered by the vertical projection of the tree canopy (Jennings, 1999). In forest management, CC is a crucial indicator for determining thinning intensity and is vital for forest stock volume estimation. The airborne forestry toolbox was used to calculate the average LAI and CC for each grid cell. The Tree Density (TD) was calculated based on the CHM segmentation results using the fishnet and spatial join tools in ArcGIS, and was defined as the number of trees per 100 square metres. All LiDAR-derived features are displayed in Table 1.

## 2.4. Modelling approach and interpretation

### 2.4.1. Scenarios with distinguished features for vegetation classification

To explore the effectiveness of three different feature combinations in improving the accuracy of land cover classification, we designed various scenarios utilizing support vector machines (SVMs) and Random Forest (RF) classifiers. The three feature combinations are as follows: (1) spectral and textural features; (2) spectral, textural, and topographic features; and (3) spectral, textural, topographic, and vegetation features. Eventually, we chose the RF classifier and completed the RF classification importance ranking of the spectral, textural, LiDAR-derived topographic, and vegetation features for the classification results under these three different scenarios.

### 2.4.2. Supervised classification and accuracy assessment

This study employs SVM and RF classifiers for supervised vegetation classification in the Yangjuangou catchment. The classification is based on field surveys, a 3D model derived from UAV aerial surveys conducted in October 2020 (Fig. 1d), and previous classification results from Wang et al. (2018), which tested the effectiveness of using high-resolution data from GF-1 in land cover classification in the Yangjuangou catchment. Wang et al. (2018) designed six experimental scenarios using multi-source remote sensing data, including MLC classification with GF-1, SVM-based spectral classification, and multi-source information classification. Their findings demonstrated that GF-1 high-resolution imagery outperformed traditional medium-resolution datasets (e.g., Landsat 8, Sentinel-2A) in land cover classification. Notably, the SVM-based multi-source approach achieved an overall accuracy of 90.5 %. However, due to satellite resolution limitations, Wang et al. (2018) classified land

**Table 1**  
List of selected LiDAR-derived features and descriptions.

Metrics	Definition	Reference
<b>Topography metrics(N = 5)</b>		
DEM	Elevation	
SLO	Slope	
ASP	Aspect	
TWI	Topographic wetness index	
DI	Direct insolation	
<b>Vegetation metrics (N = 4)</b>		
CHM	Canopy height obtained by the catchment segmentation	(Chen et al., 2006)
LAI	Half of the surface area of all leaves projected on the surface area of a unit	(Richardson et al., 2009)
CC	Percentage of vertical projection of forest canopy to forest land area	(Ma et al., 2017)
TD	Tree stems per 100 square metres	

cover into eight categories: arbour, shrub, meadow, terrace, dam, road, rural residential area, and water. In contrast, Due to the high resolution of UAV imagery, six land cover types were selected from the orthorectified UAV-based RGB imagery in our study, specifically RP, HS, AS, water, rural construction areas, dams and terraces. The sample selection adhered to principles of uniform distribution and maintaining a consistent number of samples across categories.

Supervised classification was performed under three different scenarios with varying feature combinations on the basis of the Google Earth Engine and two classification algorithms—SVM, and RF. Each scenario involved training and evaluation through 10 iterations to increase the classifier's accuracy. The final outputs included classification results and variable importance. For further analysis and application, we performed accuracy assessments by calculating the kappa coefficient, classification accuracy, and F1 score (the weighted average of precision and recall). These metrics assess the performance of SVM and RF classification models after incorporating LiDAR-derived features. Comparison of the results showed that the computational complexity of the SVM classifier is notably high. This is particularly true when the radial basis function (RBF) kernel is used, as it requires the computation of similarities between all samples, potentially leading to prolonged computation times. Additionally, large sample sizes may result in suboptimal performance of the SVM classifier during both the training and classification phases. By contrast, the RF classifier typically shows better performance when handling large datasets and high-dimensional data. This is due to its lower computational complexity, which allows it to process large datasets more efficiently and endows it with superior scalability. Overall, based on the classification accuracy metrics presented in Table 2, including the Kappa coefficient, overall accuracy, and F1-score (the weighted average of precision and recall), the RF classifier demonstrates superior performance over SVM in vegetation classification. Therefore, this study adopts RF as the optimal classifier for further investigation into the contribution of UAV-LiDAR to vegetation classification.

#### 2.4.3. Modelling of feature influence threshold effects

RF, one of the most popular machine learning models, is an ensemble learning algorithm introduced by Leo Breiman in 2001, and is designed to aggregate multiple decision trees (Breiman, 2001). The model operates by building multiple decision trees on randomly sampled subsets of the original dataset, with each tree selecting a subset of features for

splitting at its nodes. Known for its strong generalization ability and resistance to overfitting, RF performs effectively in both classification and regression tasks. In this study, it was applied to classify and explore the nonlinear relationships between key sub-features and model predictions. The study was conducted in two main steps: (1) The spectral and textural indices, and LiDAR-derived index dataset were split into training and testing sets based on random column selection, with 70 % of the data allocated to the training set and 30 % to the testing set. (2) In this study, the RF classification models were all configured with 100 decision trees ( $n_{\text{estimators}} = 100$ ), utilizing the Gini impurity criterion (criterion = "gini") to determine the optimal node splits. The feature selection strategy was set to "sqrt(n\_features)" (max\_features = "sqrt"), meaning that the square root of the total number of features was considered at each split. The model employed bootstrap sampling (bootstrap = True) to enhance diversity among trees. Additionally, the minimum number of samples required for a split was set to 2 (min\_samples\_split = 2), while the minimum number of samples required per leaf node was 1 (min\_samples\_leaf = 1), ensuring a balance between model complexity and performance. To ensure reproducibility, the random seed was fixed at 42 (random\_state = 42). An appropriate selection of parameters is beneficial for balancing model performance and complexity. This approach aims to achieve reliable classification through a well-optimized RF model, balancing predictive accuracy and generalizability.

However, relatively limited attention has been given to interpreting the results of these tree-based machine learning models. Given the widespread use of tree-based models, improving their interpretability has significant implications across various fields (Lundberg et al., 2020). Lundberg introduced SHAP (SHapley Additive exPlanations) to address the "black box" issue in machine learning models. SHAP can calculate the impact of each feature on the prediction outcome for a single instance (local interpretation) and, can reveal the importance of each feature over the entire dataset (global interpretation) by averaging across multiple instances. Luo et al. (2024) used SHAP to explain the RF model established on the basis of the relationship between human activities and the urban building environment. Inspired by this study, we apply SHAP to an RF classification model in the context of vegetation classification to investigate how the distribution of sub-eigenvalues affects the predicted categories. The framework of the vegetation classification and variable contribution analysis work is shown in Fig. 3. The model output provides a clear and intuitive display of each feature's

**Table 2**  
Comparison of classification accuracy when different feature combinations are used.

	SVM classifier			Spectral + textural + topographic			Spectral + textural + Topographic + vegetation		
	Spectral + textural			Spectral + textural + topographic			Spectral + textural + Topographic + vegetation		
	UA (%)	PA (%)	F1 (%)	UA (%)	PA (%)	F1 (%)	UA (%)	PA (%)	F1 (%)
RP	91.61	71.35	77.07	100	48.88	61.90	100	31.42	38.33
HS	65.06	95.75	73.90	52.38	100	68.01	49.12	100	65.42
AS	97.59	83.50	90.56	100	73.52	83.48	100	68.10	78.46
Water	100	98.64	99.75	100	97.84	100	100	100	100
Rural construction area	100	98.96	98.76	100	99.30	100	100	96.89	99.08
Dams and terraces	100	88.78	92.85	100	92.36	96.19	100	97.39	95.77
Overall Accuracy	88.14 %			84.84 %			80.91 %		
Kappa coefficient	85.78 %			81.82 %			76.94 %		
 Random forest classifier									
Spectral + textural			Spectral + textural + topographic			Spectral + textural + Topographic + vegetation			
RP	95.59	95.59	95.59	97.79	98.62	98.20	98.99	99.52	99.25
HS	93.56	96.69	95.10	98.05	99.14	98.59	99.62	99.55	99.58
AS	93.43	87.67	90.45	98.46	94.25	96.31	99.46	98.92	99.18
Water	100	91.89	95.77	100	90.62	95.08	100	86.67	92.85
Rural construction area	100	95.34	97.61	100	100	100	100	96.15	98.04
Dams and terraces	96.83	83.73	89.80	99.69	95.84	97.73	98.76	99.37	99.07
Overall Accuracy (%)	94.37			98.13			99.36		
Kappa coefficient (%)	91.08			97.03			99.01		

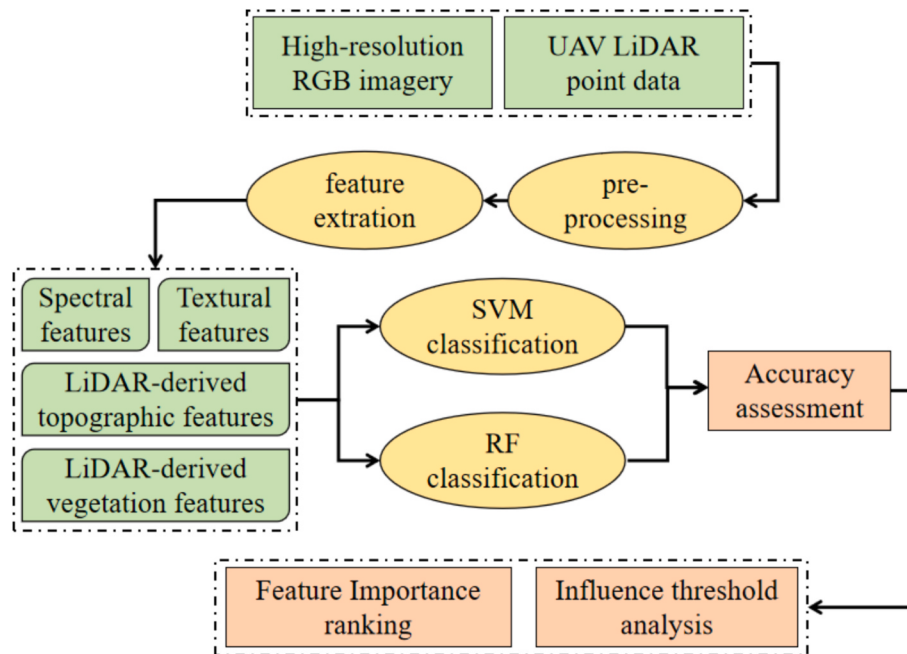


**Fig. 3.** Framework of vegetation classification and variable contribution analysis by machine learning.

importance and its effect on model performance:

$$f(x) = g(z') = \varphi_0 + \sum_{i=1}^M \varphi_i z'_i \quad (1)$$

where  $f(x)$  represents the prediction outcome of the RF classification model on the training dataset,  $g(z')$  denotes the interpretative model as a linear function specific to input  $z$ ,  $M$  is the number of input features; and  $\varphi_i$  is the contribution of the  $i$ -th feature, referred to as the SHAP value, which is defined as follows:

$$\varphi_i = \sum_{S \subseteq \{x_1, x_2, \dots, x_M\} \setminus \{x_i\}} \frac{|S|(M - |S| - 1)!}{M!} [f_x(S \cup \{x_i\}) - f_x(S)] \quad (2)$$

where  $M$  is the training dataset of feature variables used for RF classification, and  $S$  is a subset of all feature variables, and  $f_x(S)$  corresponds to the output of the RF model defined by the subset  $S$ .

### 3. Results

#### 3.1. Classification maps and accuracy evaluation

By comparing the classification accuracy and effectiveness of different feature combinations and classification methods, this study investigates the applicability of various features and classification methods in surface cover classification research in the Yangjuangou catchment. It also explores the role of LiDAR-derived features in improving classification accuracy. The classification accuracies results are shown in Table 2. With regard to overall performance, the RF classifier outperforms the SVM classifier in all aspects; therefore, in the rest of the study, we carry out an in-depth exploration of the classification results and accuracy validation of the three feature combinations in RF classification.

##### 3.1.1. SVM classification based on different feature combinations

In this study, we observed that the classification accuracy of the SVM classifier progressively decreased as more features were added across three different combinations of features. This phenomenon is consistent with the well-known concept of the ‘curse of dimensionality’ (Sammut & Webb, 2017) in machine learning, where an increase in the number of features expands the dimensionality of the data space, leading to a

decline in the performance of classifiers such as SVMs. For this study, the underlying cause of the decline may be assigned to the high computational complexity arising from the large sample size, which overwhelms the SVM’s capacity to effectively handle the integration of additional features.

In our case, the SVM classifier was first trained using spectral and textural feature data, employing a RBF kernel ( $C = 10$ ,  $\gamma = 0.001$ ) optimized through a grid search. Then, the classifier was used to generate a 1-m resolution surface cover classification map for the Yangjuangou catchment. The results, as detailed in Table 2, revealed an overall classification accuracy of 89.61 %, with a kappa coefficient of 0.87. In a subsequent model, we included additional LiDAR-derived topographic features in the SVM training. Under the same RBF kernel parameters, this model achieved an overall accuracy of 84.28 %, with a kappa coefficient of 0.81 (Table 2). Finally, the incorporation of LiDAR-derived vegetation features further decreased the overall accuracy to 81.15 %, with a corresponding kappa coefficient of 0.77, again demonstrating the adverse effects of high-dimensional feature spaces on the classification performance. These results underscore the challenges posed by increased feature dimensionality, particularly in the context of SVM-based classification.

##### 3.1.2. RF classification based on spectral and textural features

An RF classifier was trained using spectral and textural feature data. This method was used to generate a surface cover classification map of the Yangjuangou catchment with a resolution of 1 m, as depicted in Fig. 4a. The accuracy results are shown in Table 2, with the method achieving an overall accuracy of 94.37 % and a kappa coefficient of 0.91.

##### 3.1.3. RF classification based on Spectral, Textural, and LiDAR-derived topography features

The RF classifier was retrained incorporating LiDAR-derived topography features into the spectral and textural feature data. This method produced a land cover classification map of the Yangjuangou catchment with a resolution of 1 m, as illustrated in Fig. 4b. The accuracy results are presented in Table 2, with an overall accuracy of 98.13 % and a kappa coefficient of 0.97.

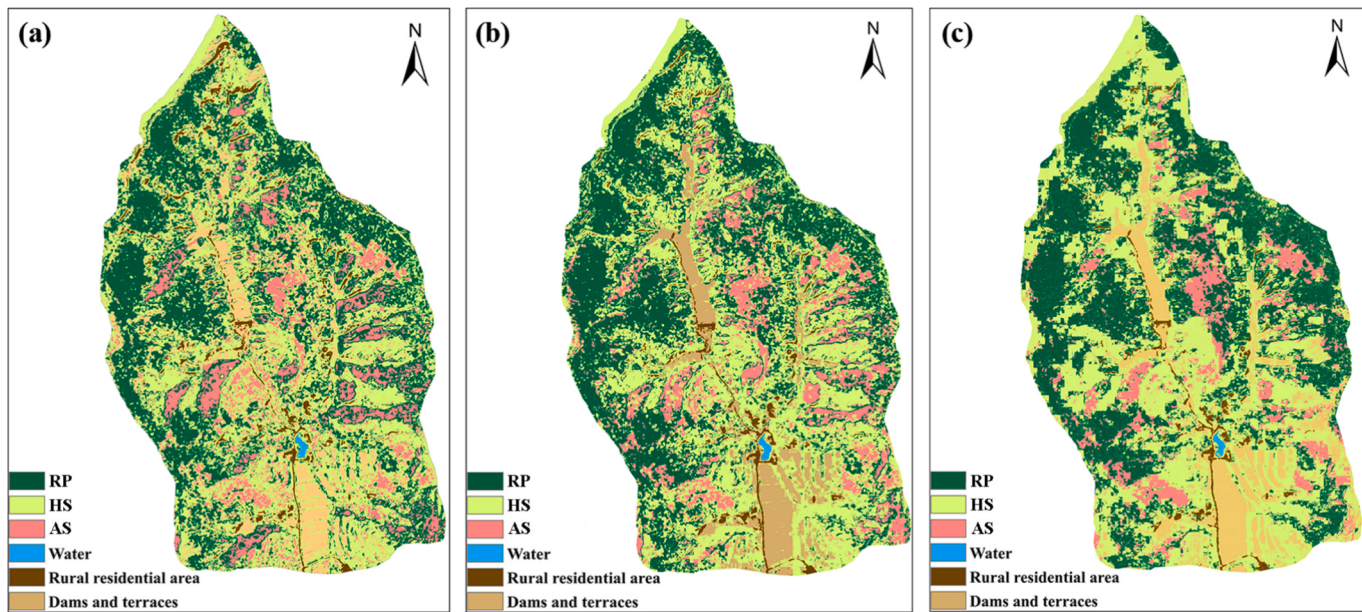


**Fig. 4.** RF classification results obtained using different combinations of features. (a) Combinations of spectral, and textural features only. (b) Combinations of spectral, textural, and LiDAR-derived topographic features. (c) Combinations of spectral, textural, and LiDAR-derived topographic features and vegetation features.

### 3.1.4. RF classification based on Spectral, Textural, LiDAR-derived Topography, and LiDAR-derived vegetation features

The RF classifier was retrained incorporating LiDAR-derived topography and vegetation features into the spectral and textural feature data. This method produced a land cover classification map of the Yang-juangou catchment with a resolution of 1 m, as illustrated in Fig. 4c. The accuracy results are presented in Table 2, with an overall accuracy of 99.36 % and a kappa coefficient of 0.99.

### 3.2. Supervised classification performance assessment

The classification and accuracy results (Table 2 and Fig. 4) indicate that integration of spectral and textural features, topographic features, and vegetation features can significantly improve the overall classification accuracy. The overall accuracy for the spectral and textural feature combination is 94.37 %, which increases to 98.13 % with the addition of topographic features, and reaches 99.36 % with the inclusion of both topographic and vegetation features. Compared with the use of only spectral and textural features, the incorporation of LiDAR-derived features provides significantly greater accuracy.

Confusion matrices, as shown in Fig. 5, offer deeper insight into the details of misclassification. When only spectral and textural features are used, there is significant misclassification among the RP, AS, and HS classes (Fig. 5a). However, these errors are significantly reduced when additional features are integrated. Specifically, the inclusion of spectral, textural, and topographic features notably reduces misclassification between the RP and HS species, and similarly minimizes the errors for the AS species. Moreover, classification errors in rural construction areas are significantly reduced when a combination of spectral, textural, and topographic features is used. By contrast, water bodies are rarely misclassified regardless of feature combinations, highlighting the robustness of their spectral signatures. The combined use of spectral, textural, topographic, and vegetation features leads to a significant reduction in both omission and misclassification errors across all categories. In particular, under the combined use of spectral, textural, topographic, and vegetation features, misclassification rates for nearly all categories are notably diminished. Finally, the optimal classification results obtained with this feature combination are presented in Fig. 4c.

### 3.3. Importance ranking of selected features

The feature importance rankings for classification, which are based on different combinations of selected spectral, textural, and LiDAR-derived data (for a total of 36 features), are presented in Fig. 6. As illustrated in Fig. 6a, b3\_savg is identified as the most important feature for the classification that combines only spectral and textural features, followed by b1\_savg and b2\_savg. In Fig. 6b, which represents the classification incorporating spectral, textural, and LiDAR-derived topographic features, DEM emerges as the most important feature. Notably, all five topographic metrics rank within the top 15 features, with DEM, SLO, and ASP as the three most important features. Fig. 6c shows the classification that integrates spectral, textural, and LiDAR-derived topography and vegetation features. In this combination, features such as DEM, CHM, SLO, and ASP are significantly more important than the other features, and occupy the top four positions. Among the top 10 features, all eight LiDAR-derived features, except for DI, play crucial roles.

The results indicate that LiDAR-derived features (including both topography and vegetation) are consistently ranked as the most important variables when they are incorporated into the classifier. Notably, topographic features, particularly SLO and ASP, demonstrate stable importance across different feature combination scenarios, highlighting the crucial role of topographic information in classification tasks. The inclusion of LiDAR data greatly improves classification accuracy, as it supplements the limitations of spectral and textural data by providing vital topographic and vegetation information. This fusion of multisource data effectively strengthens the overall model performance.

### 3.4. Influence threshold effects of features

The five most important LiDAR-derived topographic and vegetation features were selected on the basis of SHAP values to investigate the complex nonlinear relationships between these selected features and model prediction categories. By visualizing both the distribution of original feature data and the variation in SHAP values, thresholds were identified that demonstrate the influence of specific features on the model's predictions for different vegetation types (Molnar, 2020). These results aim to clarify the influence mechanisms of specific features on vegetation type predictions, thereby providing deeper insights into

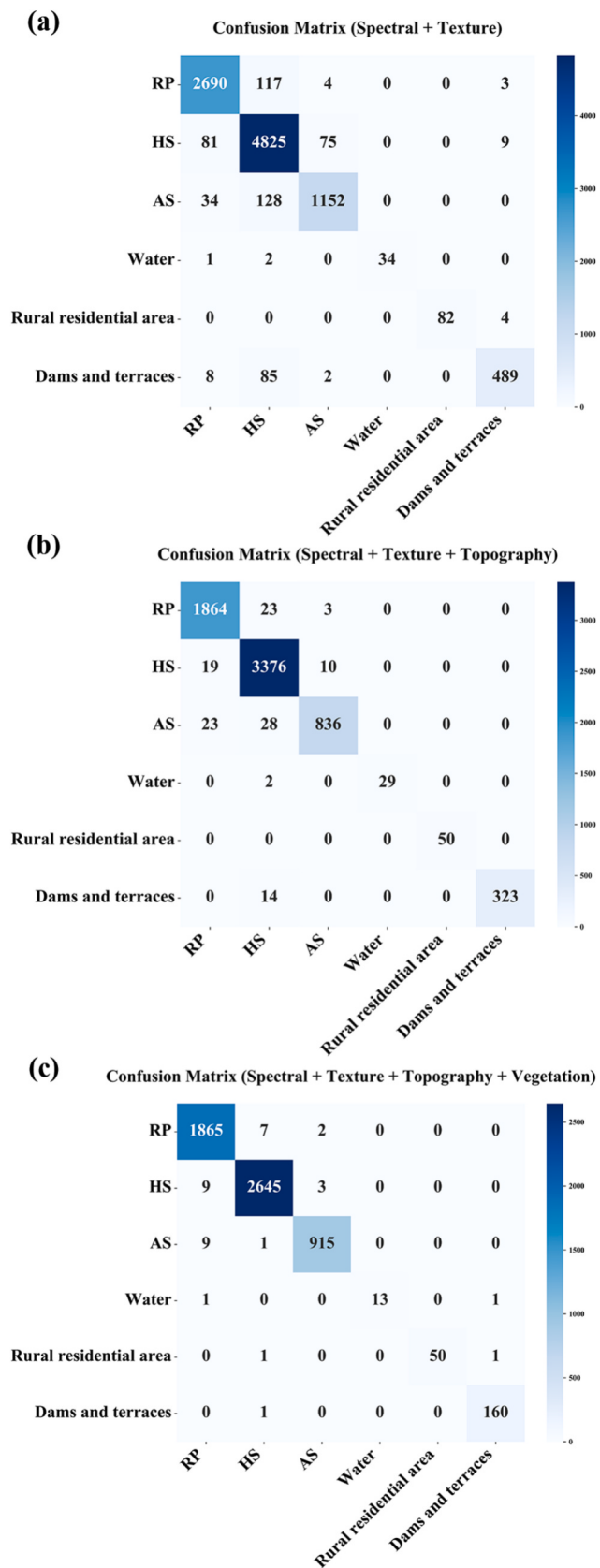


**Fig. 5.** Confusion matrix of different feature combinations in the RF classification. (a) Combinations of spectral, and textural features only. (b) Combinations of spectral, textural, and LiDAR-derived topographic features. (c) Combinations of spectral, textural, and LiDAR-derived topographic features and vegetation features.

model behaviour and feature importance. In each influence threshold plot (Fig. 8), the x-axis represents the distribution of LiDAR-derived sub-features impacting the classification outcomes, whereas the y-axis reflects the changes in the SHAP values.

### 3.4.1. Contribution of each feature to the model

SHAP values reflect the contributions of important sub-features to model prediction outcomes. A higher SHAP values indicates a greater positive contribution of a feature to the prediction, while a lower value indicates a lesser or negative contribution. Fig. 7a - c display the relative contributions of the key sub-features to the predictive modelling of RP (Category 1), AS (Category 2), and HS (Category 3), respectively. Global and local interpretations reveal distinct nonlinear and marginal effects of different features on the classification predictions for these three vegetation types. The Canopy Height Model (CHM) and Total Density (TD) are core features that significantly impact predictions across all categories. These features are particularly critical in the models predicting RP and HS, where they notably enhance the classification accuracy. For RP (Fig. 7a), the mean SHAP values for CHM and TD were approximately 0.09 and 0.07, respectively. These values highlight these features as the key factors for predicting RP. The Digital Elevation Model (DEM) also contributes to the prediction of this category, with a mean SHAP value of 0.04. For AS (Fig. 7b), CHM and TD continue to dominate, with mean SHAP values of 0.12 and 0.09, respectively. The importance of DEM increases in this category, reaching a mean SHAP value of 0.05, indicating that topographic features play a significant role in the classification of AS. For HS (Fig. 7c), textural features have a notably stronger influence. The mean SHAP values of b2\_diss and b2\_contrast reach 0.05 and 0.045, respectively, making them the most influential features for predictions. This finding indicates that textural information possesses greater discriminative power for this category. While CHM and TD have mean SHAP values of approximately 0.03 and 0.035, their relative importance is markedly lower than in Categories 1 and 2, respectively. These findings underscore the varying degrees of influence of the core features across vegetation types, highlighting the contribution of specific features in achieving accurate classifications within each category.

### 3.4.2. Threshold effects of various features on classification models

Based on the results indicated by the SHAP values, five LiDAR-derived features (ASP, CHM, DEM, SLO, TD) were ultimately selected. Using the trained RF classification model, further investigation was conducted to explore the influence patterns and threshold effects of each sub-feature on the three types of vegetation. The specific contributions of these features to the model predictions for different vegetation types are illustrated in Fig. 8. The results demonstrate that the influence patterns of these features vary significantly among different vegetation types, indicating a high degree of nonlinearity and complexity.

The analysis of contributions from various LiDAR-derived topography and vegetation features demonstrated their significant role in improving the accuracy of catchment vegetation classification. For aspect (ASP) (Fig. 8a), the SHAP values for RP and HS indicated a complex relationship. The response of RP exhibited a fluctuating negative correlation, particularly with a significant negative response on semi-sunny slopes. The SHAP values for the HS decreased on shady slopes and increased elsewhere, indicating a notably positive effect on semi-sunny slopes. By contrast, the SHAP values for AS remained stable, indicating low sensitivity to aspect. These findings highlight the importance of aspect in determining vegetation distribution patterns. The analysis of SHAP values for the Canopy Height Model (CHM) (Fig. 8b) revealed that RP had a significant positive contribution at canopy heights in the range of 5–15 m, whereas a smaller negative response was observed at lower heights. The HS exhibited a continuous decline in the SHAP contribution with increasing CHM, whereas the SHAP values for AS remained stable at lower heights (approximately 5 m), with minimal variation as height increased. These results indicate

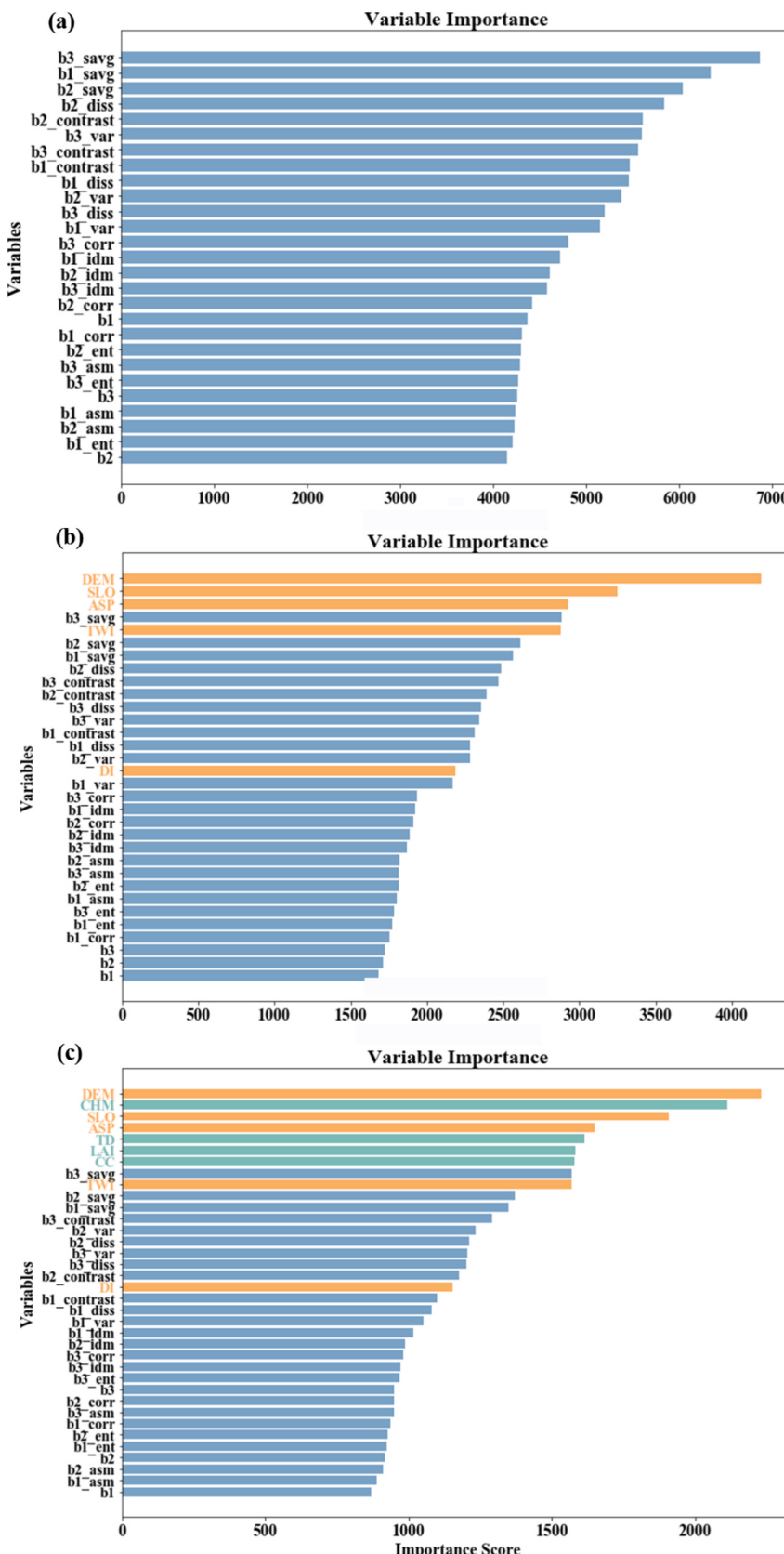


**Fig. 6.** Feature importance ranking using different feature combinations for classification, where yellow represents the topographic factor and green represents the vegetation factor. (a) Spectral and textural features only. (b) Spectral, textural, and LiDAR-derived topographic features. (c) Spectral, textural, and LiDAR-derived topographic and vegetation features.

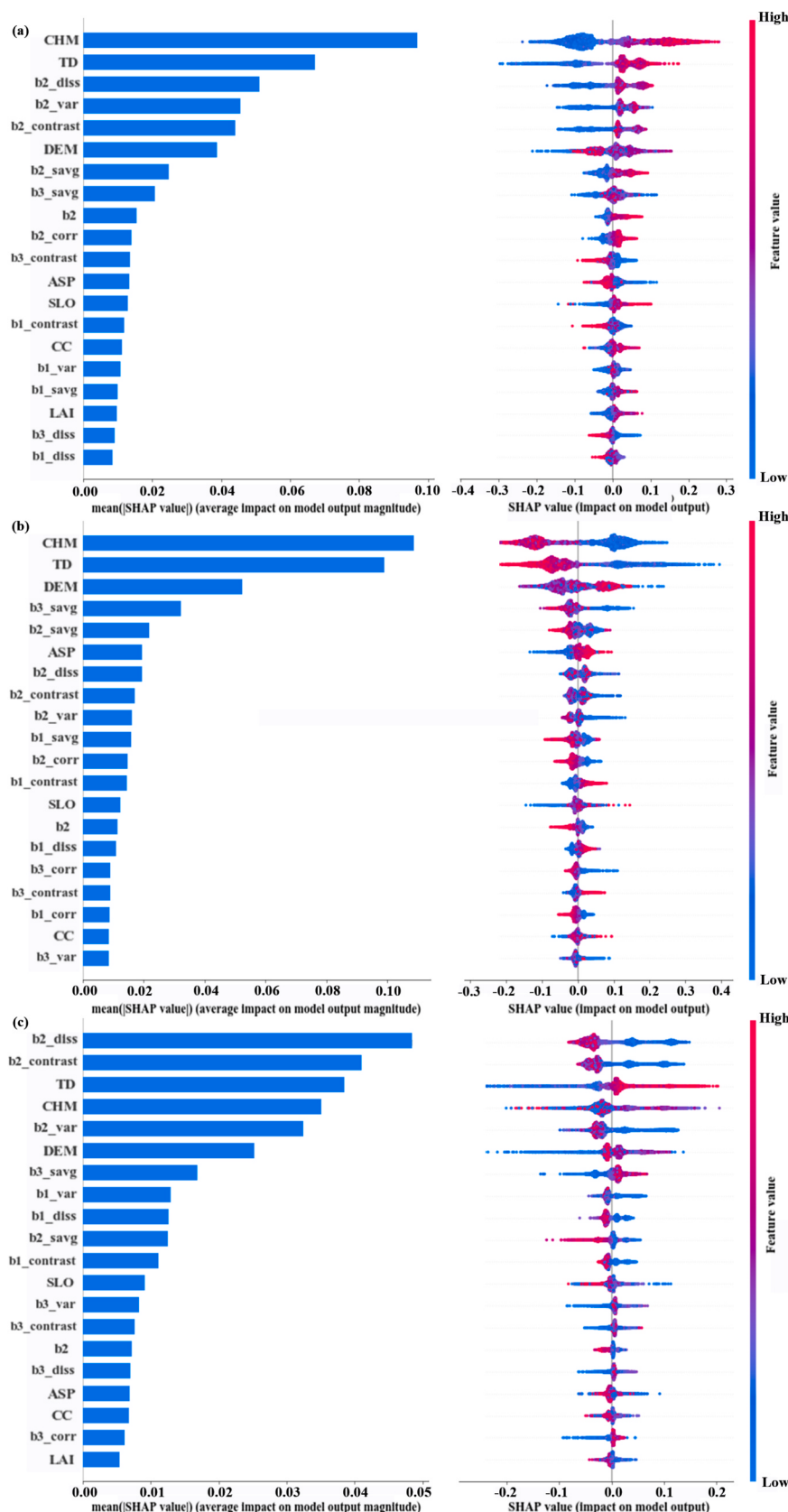
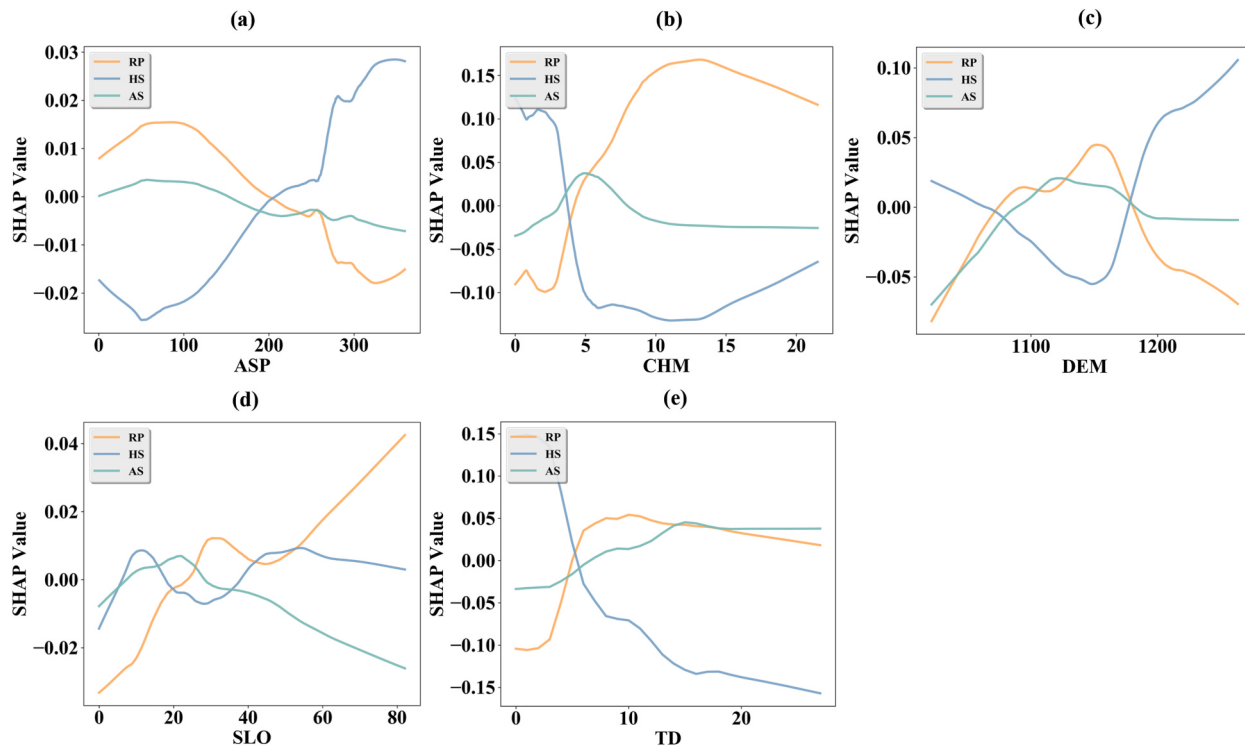


Fig. 7. Relative importance of explanatory variables in global and local interpretations: (a) Target category – RP, (b) Target category – AS, (c) Target category – HS.



**Fig. 8.** Impact threshold plots for selected LiDAR-derived features of three vegetation types. (a) Impact threshold plot for ASP. (b) Impact threshold plot for CHM. (c) Impact threshold plot for DEM. (d) Impact threshold plot for SLO. (e) Impact threshold plot for TD.

the discriminative power of the CHM in differentiating vegetation types. With regard to elevation (DEM) (Fig. 8c), the SHAP values for RP and HS tended to increase at higher elevations (above 1150 m), with the HS exhibiting the most pronounced increase in the SHAP values at high elevations. Conversely, the SHAP values for AS remained stable at lower elevations (1050–1150 m), indicating lower sensitivity to the changes in elevation. These findings were consistent with the vegetation distribution patterns observed in three-dimensional models and orthophotos obtained from drones, further validating the importance of DEM in vegetation classification. The slope (SLO) analysis (Fig. 8d) revealed that RP had a greater positive contribution to steep slopes (above 40°), suggesting a preference for steeper environments. Moreover, the HS presented greater SHAP contributions at moderate slopes (20°–40°). The SHAP values for AS generally displayed a flat response to slope, indicating no significant preference for slope conditions. The analysis of Tree Density (TD) and its relationship with the three vegetation types (Fig. 8e) revealed that the SHAP values for RP presented a positive response at low tree density, gradually turning negative with increasing density. The SHAP values for the HS decreased significantly at low to medium tree densities and remained stable in the high-density regions. AS exhibited a slight negative correlation with tree density, with contributions decreasing as the density increased. The findings highlight the complex influence patterns of various LiDAR-derived features on different vegetation types, underscoring their critical role in the classification models. To improve the accuracy and reliability of the vegetation classification models, it is essential to fully consider these nonlinear and multidimensional environmental features during modelling.

#### 4. Discussion

##### 4.1. Contributions of LiDAR-derived indicators

Recent advances in drone-based hyperspectral remote sensing and LiDAR technology have been explored as precise tools for accurate vegetation type classification at fine spatial scales (Cao et al., 2021).

Previous studies have shown that the spatial information of tree crowns derived from ALS compensates for the lack of discriminative power of spectral information, effectively providing relevant structural information for species identification (Torabzadeh et al., 2019). Scheeres et al. (2023) explored the potential of LiDAR metrics, demonstrating the ability of UAV-based LiDAR to identify complex forest structures at the plot scale, and reported that indices such as the understory leaf area index, canopy ruggedness, and an index reflecting changes in the level of the point cloud were important for distinguishing among six tropical forest restoration types. The above studies have demonstrated that vegetation attributes, such as canopy structure and leaf area index, contribute significantly to species identification. Building upon these findings, this study utilized UAV-LiDAR to extract high-resolution topographic and vegetation features while simultaneously examining their combined influence on RF classification performance. As illustrated in Fig. 7, LiDAR-derived topographic and vegetation indices, including CHM, TD, and DEM, significantly contribute to RF classification. These results highlight that the synergistic use of LiDAR-derived topographic information and vegetation parameters enhances the accuracy of vegetation classification.

Specifically, this study proposes the extraction of vegetation features such as the Canopy Height Model (CHM), Tree Density (TD), leaf area index (LAI), and Canopy Cover (CC) from LiDAR point cloud data, as well as topographic features such as the Digital Elevation Model (DEM), solar radiation index (DI), and slope (SLO). The results indicate that topographic features, primarily DEM, SLO, and ASP, along with vegetation features, mainly CHM and TD, contribute significantly to RF classification. Their integration enhances overall classification accuracy, as illustrated in Figs. 6 - 7. Moreover, this study developed a feature-layered extraction script in Google Earth Engine to systematically extract spectral, textural, topographic, and vegetation features across the entire watershed, at a 1 m × 1 m resolution. The extraction process was conducted in a single operation, using the latitude and longitude of each raster center point as an index. All feature datasets were then integrated based on their spatial coordinates, providing a direct

foundation for subsequent model training and feature contribution assessment. Tree species categorization and accuracy assessments were conducted on the basis of sample patches coded with tree species attributes. By comparing the kappa coefficient and overall accuracy metrics of the SVM and RF classifiers, we found that the RF classifier achieves the best performance when spectral features are integrated with LiDAR-derived topographic and vegetation features. The classification results are in agreement with previous research findings, indicating that the fusion of hyperspectral and LiDAR data can effectively improve classification accuracy (Qin et al., 2022), achieving high-accuracy vegetation classification with an accuracy rate exceeding 90 %.

To further examine the contribution of added topographic and vegetation features to improved classification accuracy in RF classification, we employed SHapley Additive exPlanations (SHAP) (Friedman, 2001) to visualize and quantify the impact of each feature and the changes in thresholds, thereby enhancing the interpretability of the RF model. The importance analysis of feature variables under the combination of spectral, textural, and LiDAR-derived features indicates that key extraction factors in the loess hilly and gully region primarily include CHM, TD, DEM, SLO, and ASP, which significantly contribute to improved classification accuracy. Furthermore, these indices effectively distinguish between different types of artificial vegetation, reflecting changes and thresholds across various vegetation types. Given the natural characteristics and field survey data in the study area located in the Loess Plateau's hilly and gully region, the contribution of CHM may be attributed to the significant differences among the three vegetation types: RP, AS, and HS, with the latter having the lowest height. The classification results are reasonable. Additionally, RP and AS show distinct threshold differences in canopy height, slope and aspect, as indicated by the impact threshold plots (Fig. 8), supporting the validity of the classification results. In conclusion, we observed that LiDAR-derived features have great potential for vegetation classification in complex landscapes. Previous studies highlighted the importance of LiDAR-based metrics in improving tree species classification and distinguishing forest types (Li et al., 2024; Quan et al., 2023; Scheeres et al., 2023; Torabzadeh, 2019). Building on this foundation, this study fully exploits the complementary advantages of LiDAR-derived topographic and vegetation features, offering a set of selectable feature indicators for vegetation classification in heterogeneous landscapes.

#### 4.2. Limitations and future work

The results indicated that high-precision classification of planted vegetation in this catchment is effective. The newly utilized set of LiDAR-derived metrics successfully distinguished between the two types of planted vegetation, RP and AS, as well as HS, with high accuracy. Nevertheless, some limitations still exist.

This study was conducted in a small catchment located in the hilly and gully region of the Loess Plateau, which is an area that has undergone more than seventy years of afforestation efforts. Aside from some low-lying shrubs covered by tree canopies, the vegetation in the study area primarily consists of RP, AS, and HS. The natural attributes of vegetation, such as its spatial distribution and structural characteristics, provide a basis for our classification work. For example, differences in the canopy height between herbs and shrubs and the other two types of planted vegetation, and the distinctions in the slope (SLO) shown in Fig. 8d between RP and AS, facilitate the classification process. With regard to data collection, the acquisition of high-resolution Unmanned Aerial Vehicle (UAV) imagery and LiDAR data was carried out in September and October, which is a time period when the spectral differences between RP and AS are more pronounced, thus enhancing classification accuracy. Additionally, owing to the relatively small area of the water bodies and the well-structured spatial distribution of rural construction land within the Yangjianguo catchment, these categories demonstrated high accuracy during classification validation. Future studies could further investigate the feasibility and stability of the

classification method in areas with more complex surface vegetation cover. With regard to feature extraction, this study used RGB imagery as the primary spectral feature data, which is somewhat limited in scope, comprising only the red, green, and blue bands, without spectral information in the red-edge or near-infrared bands. The use of a UAV equipped with a hyperspectral imaging sensor can provide hundreds of spectral bands and more detailed spatial information. Future classification work could leverage the advantages of hyperspectral data to increase the contribution of spectral features (Wu, 2024). In addition, with regard to data fusion, a limited number of topography and vegetation indices were derived from LiDAR. While the results demonstrated the significant contributions of the features such as the Digital Elevation Model (DEM) and Canopy Height Model (CHM), there is still room for improvement in utilizing point cloud data. For example, structural features such as tree diameter at breast height and canopy diameter, as well as point cloud distribution characteristics such as percentiles, means, and standard deviations of non-ground point heights, have been underexplored (Nie, 2017). Future work can carry out a more in-depth investigation into these features to enrich the classification index types and improve the reliability of the classification results. Additionally, we plan to validate the robustness of this classification method in more complex regions, using a broader range of datasets and metrics to improve model stability. Furthermore, future research will also explore the potential of deep learning-based point cloud understanding frameworks, such as Sen-net (Lu et al., 2025), for forest scene-level semantic segmentation, or leverage 3D-CNN architectures for capturing spatial and depth features from LiDAR point clouds. These advancements will enable more automated, scalable, and interpretable vegetation classification models, reducing reliance on manual feature engineering. Compared to traditional machine learning techniques, deep learning-based approaches offer superior adaptability to complex forest environments and large-scale ecological monitoring, making them highly suitable for future applications in forest resource assessment and environmental analysis (Mäyrä et al., 2021).

In summary, by integrating multi-resource data fusion, exploring additional LiDAR-derived structural indices, and adopting advanced deep learning architectures, future studies can further enhance the accuracy, efficiency, and applicability of tree species classification in complex forest ecosystems.

#### 5. Conclusion

This study proposes a vegetation types classification method for small catchments with complex topographies that leverages high-resolution UAV imagery and LiDAR point cloud data. Using SHAP values, the contributions of various features, particularly the LiDAR-derived features, were quantified and ranked to characterize their role in enhancing classification accuracy. The results show that in the constructed RF model, the integration of topographic and vegetation features derived from LiDAR—particularly canopy height, slope, aspect, stand density, and elevation—significantly improved classification accuracy and efficiency compared with the use of spectral and textural features only. Therefore, this method is a reliable choice for vegetation classification in the loess hilly and gully region. Impact influence analysis further revealed that topographic structure, direct solar radiation, and canopy information greatly contribute to the identification of surface vegetation and dam structures. The RF classifier, which combines spectral, textural, topographic, and vegetation features, achieved the highest classification accuracy. With regard to algorithm selection, RF outperformed SVM owing to its robustness, reduced overfitting, and efficiency in handling large, high-dimensional datasets, as well as its stability and interpretability. This method provides a reliable tool for accurate land cover and vegetation classification at the catchment scale in regions with complex topography and heterogeneous vegetation cover. Furthermore, this study also provides a basis for future studies on the ecological and environmental impacts of artificial vegetation in

different terrains.

## CRediT authorship contribution statement

**Tao Huang:** Writing – review & editing, Writing – original draft, Visualization, Validation, Methodology, Investigation, Data curation. **Lei Jiao:** Writing – review & editing, Methodology, Funding acquisition, Conceptualization. **Yingfei Bai:** Writing – review & editing. **Jianwu Yan:** Writing – review & editing. **Xiping Yang:** Writing – review & editing. **Jiayu Liu:** Writing – review & editing. **Wei Liang:** Writing – review & editing. **Da Luo:** Writing – review & editing. **Liwei Zhang:** Writing – review & editing. **Hao Wang:** Writing – review & editing. **Zhaolin Li:** Writing – review & editing. **Zongshan Li:** Writing – review & editing. **Ni Ji:** Writing – review & editing. **Guangyao Gao:** Writing – review & editing.

## Declaration of competing interest

The authors declare that they have no known competing financial interests or personal relationships that could have appeared to influence the work reported in this paper.

## Acknowledgement

This research was supported by the National Natural Science Foundation of China (NSFC) (Nos. 42271098 and U2243231) and the Natural Science Basic Research Plan in Shaanxi Province of China (2024JC-YBMS-390).

## Appendix A. Supplementary data

Supplementary data to this article can be found online at <https://doi.org/10.1016/j.compag.2025.110360>.

## Data availability

Data will be made available on request.

## References

- Belgiu, M., 2016. Random forest in remote sensing: A review of applications and future directions. *ISPRS J. Photogramm. Remote Sens.*. 114, 24–31. <https://doi.org/10.1016/j.isprsjprs.2016.01.011>.
- Breiman, L., 2001. Random forests. *Mach. Learn.* 45 (1), 5–32. <https://doi.org/10.1023/A:1010933404324>.
- Cao, J., Liu, K., Zhuo, L., Liu, L., Zhu, Y., Peng, L., 2021. Combining UAV-based hyperspectral and LiDAR data for mangrove species classification using the rotation forest algorithm. *Int. J. Appl. Earth Obs. Geoinf.* 102, 102414. <https://doi.org/10.1016/j.jag.2021.102414>.
- Caras, T., Latí, R.N., Holland, D., Dubinin, V.M., Hatib, K., Shulner, I., Keiesar, O., Liddor, G., Paz-Kagan, T., 2024. Monitoring the effects of weed management strategies on tree canopy structure and growth using UAV-LiDAR in a young almond orchard. *Comput. Electron. Agric.* 216, 108467. <https://doi.org/10.1016/j.compag.2023.108467>.
- Chen, Q., Baldocchi, D., Gong, P., Kelly, M., 2006. Isolating individual trees in a savanna woodland using small footprint lidar data. *Photogramm. Eng. Remote Sens.* 72 (8), 923–932. <https://doi.org/10.14358/PERS.72.8.923>.
- Cheng, D., 2023. Effects of species mixtures on soil water storage in the semiarid hilly gully region. *Sci. Total Environ.* 897, 165409. <https://doi.org/10.1016/j.scitotenv.2023.165409>.
- Chrysafis, I., Mallinis, G., Tsakiri, M., Patias, P., 2019. Evaluation of single-date and multi-seasonal spatial and spectral information of Sentinel-2 imagery to assess growing stock volume of a Mediterranean forest. *Int. J. Appl. Earth Obs. Geoinf.* 77, 1–14. <https://doi.org/10.1016/j.jag.2018.12.004>.
- Corte, A.P.D., Souza, D.V., Rex, F.E., Sanquette, C.R., Mohan, M., Silva, C.A., Zambrano, A.M.A., Prata, G., Alves De Almeida, D.R., Trautenmüller, J.W., Klauber, C., De Moraes, A., Sanquette, M.N., Wilkinson, B., Broadbent, E.N., 2020. Forest inventory with high-density UAV-Lidar: Machine learning approaches for predicting individual tree attributes. *Comput. Electron. Agric.* 179, 105815. <https://doi.org/10.1016/j.compag.2020.105815>.
- Fasnacht, F.E., Latí, H., Lefsky, M., Waser, L.T., Straub, C., Ghosh, A., 2016. Review of studies on tree species classification from remotely sensed data. *Remote Sens. Environ.* 186, 64–87. <https://doi.org/10.1016/j.rse.2016.08.013>.
- Fauvel, M., Tarabalka, Y., Benediktsson, J.A., Chanussot, J., Tilton, J.C., 2013. Advances in spectral-spatial classification of hyperspectral images. *Proc. IEEE*. 101 (3), 652–675. <https://doi.org/10.1109/JPROC.2012.2197589>.
- Fernández-Martínez, M., Vicca, S., Janssens, I.A., Luyssaert, S., Campioli, M., Sardans, J., Estiarte, M., Peñuelas, J., 2014. Spatial variability and controls over biomass stocks, carbon fluxes, and resource-use efficiencies across forest ecosystems. *Trees*. 28 (2), 597–611. <https://doi.org/10.1007/s00468-013-0975-9>.
- Friedman, J.H., 2001. Greedy function approximation: a gradient boosting machine. *Ann. Stat.* 29 (5), 1189–1232. <https://doi.org/10.1214/aos/1013203451>.
- Gower, S.T., Kucharki, C.J., Norman, J.M., 1999. Direct and indirect estimation of leaf area index, fAPAR, and net primary production of terrestrial ecosystems. *Remote Sens. Environ.* 70 (1), 29–51. [https://doi.org/10.1016/S0034-4257\(99\)00056-5](https://doi.org/10.1016/S0034-4257(99)00056-5).
- Hovi, A., 2014. Real and simulated waveform-recording LiDAR data in juvenile boreal forest vegetation. *Remote Sens. Environ.* 140, 665–678. <https://doi.org/10.1016/j.rse.2013.10.003>.
- Molnar, C. (2020). *Interpretable Machine Learning*. Leanpub. <https://christophm.github.io/interpretable-ml-book/>.
- Lambin, E.F., Meyfroidt, P., 2011. Global land use change, economic globalization, and the looming land scarcity. *Proc. Natl. Acad. Sci.* 108 (9), 3465–3472. <https://doi.org/10.1073/pnas.1100480108>.
- Li, X., Wang, L., Guan, H., Chen, K., Zang, Y., Yu, Y., 2024. Urban tree species classification using UAV-based multispectral images and LiDAR point clouds. *Journal of Geovisualization and Spatial Analysis*. 8 (1), 5. <https://doi.org/10.1007/s41651-023-00167-9>.
- Li, X., Jiao, L., Cheng, D., Liu, J., Li, Z., Wang, C., He, X., Cao, Y., Gao, G., 2024. Light thinning effectively improves forest soil water replenishment in water-limited areas: observational evidence from *Robinia pseudoacacia* plantations on the Loess Plateau, China. *J. Hydrol.* 637, 131408. <https://doi.org/10.1016/j.jhydrol.2024.131408>.
- Lu, H., Li, B., Yang, G., Fan, G., Wang, H., Pang, Y., Wang, Z., Lian, Y., Xu, H., Huang, H., 2025. Towards a point cloud understanding framework for forest scene semantic segmentation across forest types and sensor platforms. *Remote Sens. Environ.* 318, 114591. <https://doi.org/10.1016/j.rse.2024.114591>.
- Lundberg, S.M., Erion, G., Chen, H., DeGrave, A., Prutkin, J.M., Nair, B., Katz, R., Himmelfarb, J., Bansal, N., Lee, S.-I., 2020. From local explanations to global understanding with explainable AI for trees. *Nat. Mach. Intell.* 2 (1), 56–67. <https://doi.org/10.1038/s42429-019-0138-9>.
- Luo, L., Yang, X., Chen, X., Liu, J., An, R., Li, J., 2024. Nonlinear influence of the built environment on the attraction of the third activity: a comparative analysis of inflow from home and work. *International Journal of Geo-Information*. 13 (9), 337. <https://doi.org/10.3390/ijgi13090337>.
- Ma, Q., Su, Y., Guo, Q., 2017. Comparison of canopy cover estimations from airborne LiDAR, aerial imagery, and satellite imagery. *IEEE J. Sel. Top. Appl. Earth Obs. Remote Sens.* 10 (9), 4225–4236. <https://doi.org/10.1109/JSTARS.2017.2711482>.
- Mäyrä, J., Keski-Saari, S., Kivinen, S., Tanhuapää, T., Hurskainen, P., Kullberg, P., Poikolainen, L., Viinikka, A., Tuominen, S., Kumpula, T., Vihervaara, P., 2021. Tree species classification from airborne hyperspectral and LiDAR data using 3D convolutional neural networks. *Remote Sens. Environ.* 256, 112322. <https://doi.org/10.1016/j.rse.2021.112322>.
- Nie, S., 2017. Above-ground biomass estimation using airborne discrete-return and full-waveform LiDAR data in a coniferous forest. *Ecol. Ind.* 78, 221–228. <https://doi.org/10.1016/j.ecolind.2017.02.045>.
- Oehmcke, S., 2024. Deep point cloud regression for above-ground forest biomass estimation from airborne LiDAR. *Remote Sens. Environ.* 302, 113968. <https://doi.org/10.1016/j.rse.2023.113968>.
- Qin, H., Zhou, W., Yao, Y., Wang, W., 2022. Individual tree segmentation and tree species classification in subtropical broadleaf forests using UAV-based LiDAR, hyperspectral, and ultrahigh-resolution RGB data. *Remote Sens. Environ.* 280, 113143. <https://doi.org/10.1016/j.rse.2022.113143>.
- Quan, Y., Li, M., Hao, Y., Liu, J., Wang, B., 2023. Tree species classification in a typical natural secondary forest using UAV-borne LiDAR and hyperspectral data. *Giscience & Remote Sensing* 60 (1), 2171706. <https://doi.org/10.1080/15481603.2023.2171706>.
- Richardson, J.J., Moskal, L.M., Kim, S.-H., 2009. Modeling approaches to estimate effective leaf area index from aerial discrete-return LIDAR. *Agric. For. Meteorol.* 149 (6–7), 1152–1160. <https://doi.org/10.1016/j.agrmet.2009.02.007>.
- Sammut, C., Webb, G. I. (Eds.). (2017). *Encyclopedia of Machine Learning and Data Mining (2nd ed.)*. Springer. Doi: 10.1007/978-1-4899-7685-7.
- Scheeres, J., De Jong, J., Brede, B., Brancalion, P.H.S., Broadbent, E.N., Zambrano, A.M. A., Gorgens, E.B., Silva, C.A., Valbuena, R., Molin, P., Stark, S., Rodrigues, R.R., Santoro, G.B., Resende, A.F., De Almeida, C.T., De Almeida, D.R.A., 2023. Distinguishing forest types in restored tropical landscapes with UAV-borne LIDAR. *Remote Sens. Environ.* 290, 113533. <https://doi.org/10.1016/j.rse.2023.113533>.
- Seibert, J., Stendahl, J., Sorensen, R., 2007. Topographical influences on soil properties in boreal forests. *Geoderma*. 141 (1–2), 139–148. <https://doi.org/10.1016/j.geoderma.2007.05.013>.
- Torabzadeh, H., 2019. Tree species classification in a temperate mixed forest using a combination of imaging spectroscopy and airborne laser scanning. *Agric. For. Meteorol.* 279, 107744. <https://doi.org/10.1016/j.agrmet.2019.107744>.
- Wang, L., 2024. Individual tree species classification using low-density airborne multispectral LiDAR data via attribute-aware cross-branch transformer. *Remote Sens. Environ.* 315, 114456. <https://doi.org/10.1016/j.rse.2024.114456>.
- Wang, X., Zhou, C., Feng, X., Cheng, C., Fu, B., 2018. Testing the efficiency of using high-resolution data from GF-1 in land cover classifications. *IEEE J. Sel. Top. Appl. Earth Obs. Remote Sens.* 11 (9), 3051–3061. <https://doi.org/10.1109/JSTARS.2018.2850888>.

- Wu, J., 2024. A novel framework combining band selection algorithm and improved 3D prototypical network for tree species classification using airborne hyperspectral images. *Comput. Electron. Agric.*. 219, 108813. <https://doi.org/10.1016/j.compag.2024.108813>.
- Yue, C., Ciais, P., Houghton, R.A., Nassikas, A.A., 2020. Contribution of land use to the interannual variability of the land carbon cycle. *Nat. Commun.*. 11 (1), 3170. <https://doi.org/10.1038/s41467-020-16953-8>.
- Zhang, Y., 1999. Optimisation of building detection in satellite images by combining multispectral classification and texture filtering. *ISPRS J. Photogramm. Remote Sens.*. 54 (1), 50–60. [https://doi.org/10.1016/S0924-2716\(98\)00027-6](https://doi.org/10.1016/S0924-2716(98)00027-6).
- Zhu, W., Yang, X., Liu, R., Zhao, C., 2024. A new feature extraction algorithm for measuring the spatial arrangement of texture Primitives: distance coding diversity. *Int. J. Appl. Earth Obs. Geoinf.* 127, 103698. <https://doi.org/10.1016/j.jag.2024.103698>.